METTL3 Promotes Tumorigenesis and Metastasis through BMI1 m^{6}A Methylation in Oral Squamous Cell Carcinoma

Lin Liu,[1,9] Yu Wu,[1,9] Qiuli Li,[2,9] Jianfeng Liang,[3] Qianting He,[1] Luodan Zhao,[4] Jianwen Chen,[5] Maosheng Cheng,[6] Zhexun Huang,[1] Hui Ren,[1] Jie Chen,[1] Liang Peng,[7] Fengxin Gao,[8] Demeng Chen,[5] and Anxun Wang[1]

[1]Department of Oral and Maxillofacial Surgery, First Affiliated Hospital, Sun Yat-Sen University, Guangzhou 510080, China; [2]Department of Head and Neck Surgery, Sun Yat-sen University Cancer Center, State Key Laboratory of Oncology in South China, Collaborative Innovation Center for Cancer Medicine, Guangzhou 510060, China; [3]Department of Oral and Maxillofacial Surgery, Guanghua School of Stomatology, Hospital of Stomatology, Sun Yat-Sen University, Guangzhou 510080, China; [4]Department of Stomatology, Sun Yat-Sen Memorial Hospital, Sun Yat-Sen University, Guangzhou 510120, China; [5]Department of Otolaryngology, Center for Translational Medicine, Precision Medicine Institute, First Affiliated Hospital, Sun Yat-sen University, Guangzhou 510080, China; [6]Department of Genetics, School of Life Science, Anhui Medical University, Anhui 230031, China; [7]Department of Oncology, Chinese PLA General Hospital, Beijing 100853, China; [8]Guangzhou Epibiotek Co., Ltd, Guangzhou 510700, China

RNA modification plays an essential function in regulating gene expression and diverse biological processes. RNA modification enzyme methyltransferase-like 3 (METTL3) affects tumor progression by regulating the N^6-methyladenosine (m^{6}A) modification in the mRNAs of critical oncogenes or tumor suppressors, but its effect in oral squamous cell carcinoma (OSCC) remains unknown. In this study, we revealed that METTL3 was consistently upregulated in two OSCC cohorts, and high METTL3 expression was associated with poor prognosis. Functionally, cell proliferation, self-renewal, migration, and invasion ability *in vitro* and tumor growth and metastasis *in vivo* were decreased after METTL3 knockdown in OSCC cells. In contrast, the opposite results were obtained after METTL3 overexpression. In addition, the results obtained with the *Mettl3* genetically modified mouse model validated the essential role of *Mettl3* in chemical-induced oral carcinogenesis. In mechanism, methylated RNA immunoprecipitation sequencing (MeRIP-seq), MeRIP-quantitative real-time PCR, and luciferase reporter and mutagenesis assays identified that METTL3 mediates the m^{6}A modification in the 3′ UTR of *BMI1* mRNA. METTL3 promotes *BMI1* translation in OSCC under the cooperation with m^{6}A reader IGF2BP1. Our findings revealed that METTL3 promotes OSCC proliferation and metastasis through *BMI1* m^{6}A methylation, suggesting that the METTL3-m^{6}A-BMI1 axis may serve as a prognostic biomarker or therapeutic target in patients with OSCC.

INTRODUCTION

Oral squamous cell carcinoma (OSCC) is the most common malignant tumor of the oral cavity. Although comprehensive treatments, including surgical treatment, radiotherapy, and chemotherapy, have made progress over the years, the prognosis of OSCC patients remains poor, and the 5-year survival rate has not been significantly improved.[1–3] Thus, clarification of the molecular mechanisms underlying OSCC invasion and metastasis is crucial to improve patient prognosis and develop effective targeted therapeutic inventions. To date, many genetic and epigenetic changes had been found to be involved in the development of OSCC. In our previous studies,[4–6] many epigenetic alterations, such as miR-21, miR-138, miR-181a, and miR-222, were verified to regulate the invasion and metastasis of OSCC through different signaling pathways. To date, few reports have focused on the m^{6}A methylation modification and OSCC.

N6-methyladenosine (m^{6}A) is the most abundant modification in mRNA and is regulated by m^{6}A methyltransferases, demethylases, and readers.[7] Methyltransferase-like 3 (METTL3), the main RNA methyltransferase, together with its auxiliary partners METTL14 and WTAP, forms a methyltransferase complex to catalyze the m^{6}A modification.[8,9] Alternatively, the demethylases FTO and ALKBH5 remove m^{6}A from mRNA to dynamically regulate the m^{6}A modification.[10,11] In addition, m^{6}A readers, including the YTH family proteins, IGF2BPs, and eIF3s, can specifically recognize m^{6}A modification and regulate the splicing, transport, translation, stability, and other functions of the downstream mRNA.[12–14] The m^{6}A modification is involved in nearly all crucial biological processes, such as proliferation and differentiation of stem cells,[15] the circadian clock,[16] spermatogenesis,[17] and tissue development.[18] Abnormal m^{6}A methylation was found to be closely related
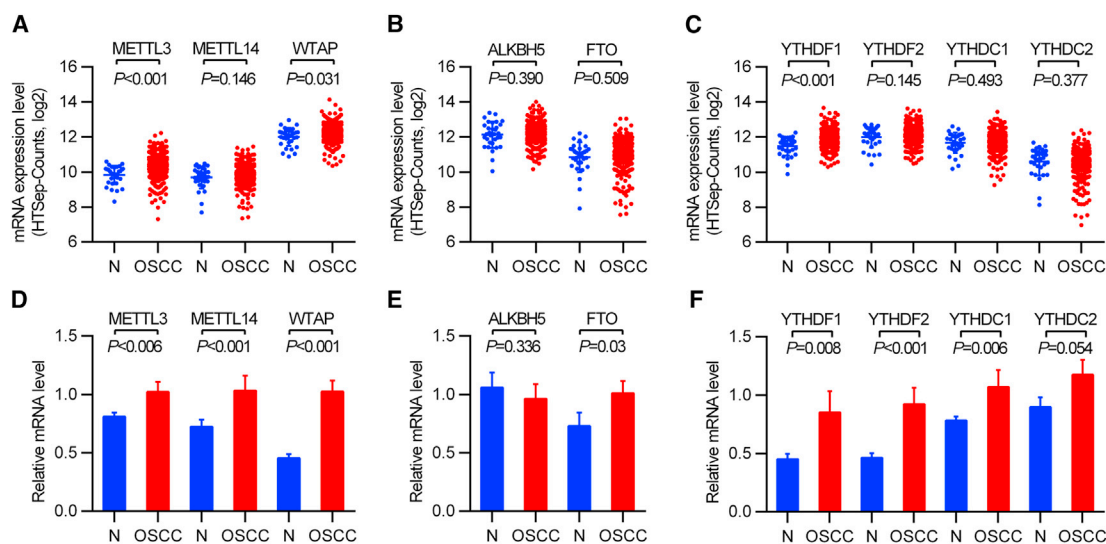
Figure 1. Deregulation of m⁶A Methylation Enzymes in OSCC

(A–F) TCGA data shown that (A) writers, METTL3, and WTAP were significantly upregulated in OSCC, while METTL14 expression was unchanged; (B) erasers, FTO, or ALKBH5 exhibited no significant changes in OSCC and normal tissues; and (C) readers and YTHDF1 were upregulated in OSCC, while YTHDF2, YTHDC1, and YTHDC2 exhibited no significant changes in OSCC and normal tissues. Quantitative real-time PCR of OSCC tissues and adjacent normal oral mucosa tissues confirmed that (D) writers, METTL3, METTL14, and WTAP were uprugulated in OSCC; (E) erasers and FTO were significantly upregulated in OSCC, while ALKBH5 expression was unchanged; and (F) readers, YTHDF1, YTHDF2, and YTHDC1 (except YTHDC2) were significantly upregulated in OSCC.

to the occurrence and development in many tumors, such as glioblastoma,[19] lung cancer,[20] breast cancer,[21] liver cancer,[22] and acute myeloid leukemia.[23] Many researchers have also found that m⁶A methylation-related proteins present different expression patterns and functions in different malignant tumors.[24,25] However, the role of m⁶A modification in OSCC remains unknown.

To investigate the functional role and underlying molecular mechanism of the m⁶A RNA methyltransferase METTL3 in the development of OSCC, first, the METTL3 expression level was analyzed in OSCC cohorts using The Cancer Genome Atlas (TCGA) database, quantitative real-time PCR, and immunohistochemistry. METTL3 was found to be consistently upregulated, and high METTL3 expression was associated with the prognosis of OSCC patients. Next, the functional role of METTL3 was investigated *in vitro* and *in vivo*, and the results verified that METTL3 promoted proliferation, self-renewal, and metastasis of OSCC. Furthermore, methylated RNA immunoprecipitation sequencing (MeRIP-seq), MeRIP-quantitative real-time PCR, and luciferase reporter and mutagenesis assays were involved and identified that METTL3 mediates the m⁶A modification in the 3′ UTR of *BMI1* mRNA. METTL3 promoted *BMI1* translation at the posttranscriptional level in OSCC under cooperation with m⁶A reader IGF2BP1. Thus, these data revealed a new epigenetic mechanism in OSCC, which has important application value in OSCC diagnosis, prognosis, and molecular-targeted therapy.

RESULTS

Deregulation of m⁶A Methylation Enzymes in OSCC

First, we compared and analyzed the expression level of the major m⁶A methylation-related modifying enzymes in 32 normal and 340 OSCC tissues from TCGA RNA sequencing (RNA-seq) database (TCGA Database: https://portal.gdc.cancer.gov/) and found that *METTL3* and *WTAP* were significantly upregulated in OSCC, while *METTL14* expression was unchanged (Figure 1A). The demethylases (*FTO* or *ALKBH5*) and m⁶A-related reading proteins (except *YTHDF1*) exhibited no significant changes (Figures 1B and 1C). To further confirm the expression of m⁶A methylation modification enzymes in OSCC, quantitative real-time PCR was performed in OSCC and its adjacent normal oral mucosa tissues, and the results showed that *METTL3*, *METTL14*, *WTAP*, *FTO*, *YTHDF1*, *YTHDF2*, and *YTHDC1* were expressed at significantly higher levels in OSCC, while *ALKBH5* and *YTHDC2* showed no significant changes (Figures 1D–1F; Figure S1). Thus, we speculated that the occurrence of OSCC may be related to deregulation of m⁶A methylation enzymes, especially upregulation of *METTL3*.

METTL3 Was Upregulated and Is Associated with Poor Prognosis in OSCC

To identify the role of METTL3 in OSCC development, immunohistochemical (IHC) staining was carried out in two OSCC cohorts. For the training sample set, METTL3 was found to be expressed in the nucleus, and its expression was rarely detectable in normal mucosa tissues but was pronounced in OSCC tissues (Figure 2A). A higher METTL3 expression level was significantly positively associated with advanced tumor stage (T_{3+4} versus T_{1+2}), advanced clinical stage (C_{III+IV} versus C_{I+II}), and lymph node metastasis (LN_+ versus LN_-), but no differences in other features, such as sex and age, were observed (Figure 2B; Table S1). Kaplan-Meier analysis of survival data revealed that the overall survival time of patients with high
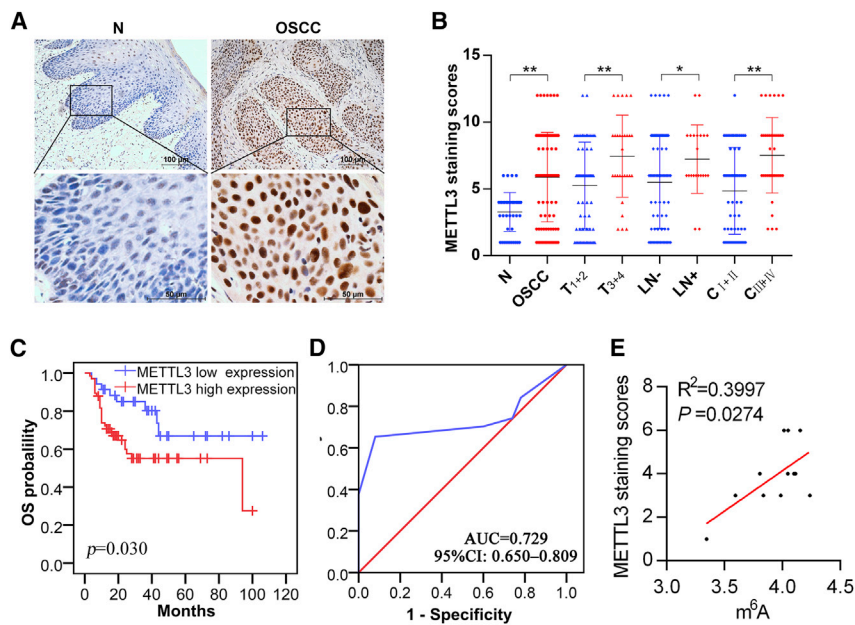
Figure 2. METTL3 Was Upregulated and Associated with Poor Prognosis in OSCC Patients

(A) IHC staining for METTL3 in a training sample composed of 101 OSCC tissue samples and 50 adjacent non-cancerous samples. (B) Statistical analysis (chi-square test) of METTL3 IHC staining scores in normal oral mucosa tissue (N) and OSCC tissues stratified by tumor stage (T_{3+4} versus T_{1+2}), clinical stage (C_{III+IV} versus C_{I+II}), and lymph node metastasis (LN_+ versus LN_-). (C) Kaplan-Meier survival curves of 5-year overall survival (OS) based on METTL3 expression level. (D) ROC curves analyzing the potential value of METTL3 expression level in OSCC diagnosis. (E) The correlation between the METTL3 protein level and total m^6A in OSCC tissue was analyzed by a Spearman's test. *$p < 0.05$, **$p < 0.01$.

(HOK) cells. Moreover, based on our previous microarray data,[26] we found that the higher migration and invasion ability of OSCC cells were correlated with a higher METTL3 expression level (Figure S4).

METTL3 expression was significantly shorter than that of patients with low METTL3 expression (Figure 2C). To further evaluate the association between the METTL3 expression level and clinicopathological factors with the prognosis of OSCC patients, univariate and multivariate analyses were conducted. As shown in Table S2, both the univariate and multivariate analyses indicated that the level of METTL3 expression is a prognostic factor for the 5-year overall survival of patients with OSCC. Moreover, the potential value of the METTL3 expression level for OSCC diagnosis was evaluated with a receiver operating characteristic (ROC) curve. As shown in Figure 2D and Table S3, the area under the curve (AUC) for METTL3 was 0.729 (95% confidence interval [CI]: 0.650–0.809), with a sensitivity of 65.3% and specificity of 92%. A cutoff value of 5 was used to differentiate patients with OSCC from healthy controls.

For the validation sample set (Figure S2; Table S4), IHC staining confirmed that OSCC tissue showed significantly higher METTL3 expression than did normal tissues, and higher METTL3 expression was again associated with advanced tumor stage (T_{3+4} versus T_{1+2}), advanced clinical stage (C_{III+IV} versus C_{I+II}), and lymph node metastasis (LN_+ versus LN_-).

Moreover, a significant correlation between the METTL3 protein level (by IHC) and total m^6A level (by dot blot) was found in six pairs of human OSCC and adjacent non-cancerous samples tissues (Figure 2E).

METTL3 Promoted OSCC Cell Proliferation, Self-Renewal, Migration, and Invasion *In Vitro*

First, the METTL3 expression level was detected in four OSCC cell lines via western blotting and quantitative real-time PCR (Figures S3A–S3C), and OSCC cells were found to exhibit higher METTL3 expression than in human normal oral epithelial keratinocyte

To investigate the functional role of METTL3 in OSCC, METTL3 knockdown models in SCC9 cells were established using lentiviruses constructed with *METTL3* short hairpin RNA (shRNA) sequences. The silencing efficacy showed that METTL3 was successfully knocked down at both the protein and mRNA levels (Figure 3A). After stable knockdown of METTL3, SCC9 cells displayed decreased proliferative capacity in a time-dependent manner (Figure 3B), decreased migration and invasion ability (Figure 3C; Figure S5A), reduced colony formation (Figure 3D), and formed fewer and smaller spheres (Figure 3E).

Alternatively, a METTL3 overexpression system was also constructed using lentivirus to explore the functional role of METTL3 in OSCC. The upregulation of METTL3 was verified at both the protein and mRNA levels (Figure 3F). Upregulation of METTL3 in SCC9 cells enhanced their proliferation capacity (Figure 3G) and migration and invasion ability (Figure 3H; Figure S5B). The colony formation ability (Figure 3I) and sphere formation ability (Figure 3J) were also significantly enhanced in the METTL3 overexpression SCC9 cells.

Moreover, similar function roles of METTL3 in another OSCC cell line (UM1) were confirmed, including proliferation, clone formation, and migration and invasion ability, as shown in Figure S6.

METTL3 Promoted OSCC Tumor Growth and Metastasis *In Vivo*

To investigate the cancer-promoting role of METTL3 *in vivo*, we subcutaneously injected the METTL3 knockdown cells and non-targeted shRNA control cells into nude mice. As shown in Figure 4A, the volume and weight of the tumors formed in the METTL3 stable knockdown group were significantly lower than those of tumors in the group treated with control shRNA, and knockdown of
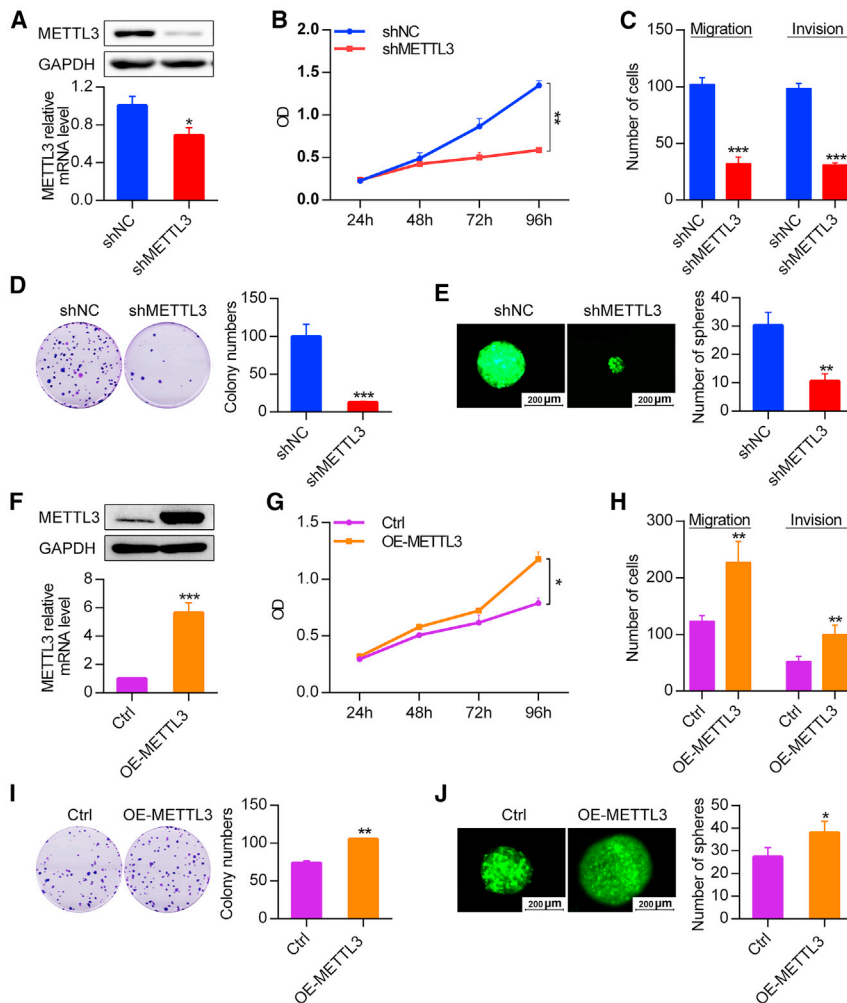
Figure 3. METTL3 Promotes OSCC Proliferation, Self-Renewal, Migration, and Invasion *In Vitro*

(A) METTL3 knockdown effect was verified by western blotting (upper panel) and quantitative real-time PCR (lower panel). (B–E) Knockdown of METTL3 reduced the proliferation ability (B), suppressed the migration and invasion abilities (C), and impaired the colony formation (D) and sphere formation (E) abilities of SCC9 cells. (F) Upregulation of METTL3 was confirmed at both the protein (upper panel) and mRNA (lower panel) levels after infection with lentivirus containing *METTL3* cDNA. (G–J) Overexpression of METTL3 increased the cell proliferation ability (G), enhanced the migration and invasion abilities (H), and promoted the colony formation (I) and sphere formation (J) abilities of SCC9 cells. $*p < 0.05$, $**p < 0.01$, $***p < 0.001$. shNC and shMETTL3, lentiviral vectors containing control shRNA or *METTL3* shRNA; Ctrl and OE-METTL3, lentiviral vectors containing control cDNA or *METTL3* cDNA.

METTL3 overexpression significantly increased lymph node metastasis; the incidence of lymph node metastasis increased by 133%. Therefore, based on the above results, we conclude that METTL3 may act as an oncogene and promote OSCC growth and metastasis.

Mettl3 Knockout (KO) in Mouse Oral Epithelia Led to Decreased Susceptibility to OSCC Carcinogenesis

To further verify the carcinogenic role of METTL3 *in vivo*, we crossed *Mettl3*$^{fl/fl}$ mice with *K14CreER* mice to generate a tamoxifen-mediated conditional *Mettl3* gene KO mouse model. First, to examine whether loss of *Mettl3* prevents or reduces 4-nitroquinoline 1-oxide (4NQO)-induced OSCC carcinogenesis in mice, *Mettl3*^{cKO} and *Mettl3*^{Ctrl} mice were injected with tamoxifen before 4NQO administration. Mice were euthanized 22 weeks after the initial 4NQO treatment (Figure 5A). We quantified the number and area of lesions in the oral cavity per mouse and classified these lesions as mild to severe dysplasia or squamous cell carcinoma. In this model, we found that control mice developed OSCC with 100% penetrance (6/6), and only 33.3% (2/6) of *Mettl3*^{cKO} mice developed mild dysplasia, indicating that loss of *Mettl3* can reduce the incidence of OSCC *in vivo*. In addition, we examined the expression of Ki67 in both groups and found that Ki67 was inhibited in the *Mettl3*^{cKO} OSCC group compared with the control group (Figure 5B). No obvious histological abnormalities were found in *Mettl3*^{cKO} mice. We next studied whether loss of *Mettl3* can suppress OSCC progression. Tamoxifen was given to *Mettl3*^{cKO} and *Mettl3*^{Ctrl} mice after 16 weeks of 4NQO treatment, when OSCC had formed in the mice. Mice were harvested at 22 weeks after 4NQO treatment (Figure 5D). The number and size of the intraoral tumors from mice were determined. Our results demonstrated that the number of clinical visible lesions in the oral cavity in *Mettl3*^{Ctrl} and *Mettl3*^{cKO} mice was 2.9 ± 1.0

METTL3 expression inhibited tumor growth by 80% at day 28 after transplantation. The doubling times for tumors derived from control shRNA-infected cells and *METTL3* shRNA-infected SCC9 cells were 5.1 and 9.7 days, respectively. In a lung metastasis model, mice injected with *METTL3* shRNA-infected cells exhibited a significantly reduced number of metastatic nodules compared with mice injected with control shRNA-infected cells (Figure 4B). Alternatively, we also injected METTL3-overexpressing cells and mock-infected cells into the subcutaneous space in nude mice and found that the volume and weight of the tumors in the METTL3 overexpression group were significantly higher than those in the control group (Figure 4C). The doubling times for tumors in the control group and METTL3 overexpression group were 5.3 and 4.3 days, respectively. The lung metastasis model also showed that overexpression of METTL3 resulted in significantly increased metastatic nodules in the lung compared with the control group (Figure 4D). Moreover, in a lymph node metastasis model (Figure 4E), METTL3 knockdown resulted in a significant reduction in lymph node metastasis; the lymph node metastasis inhibition rate was 75% relative to the control group. However,
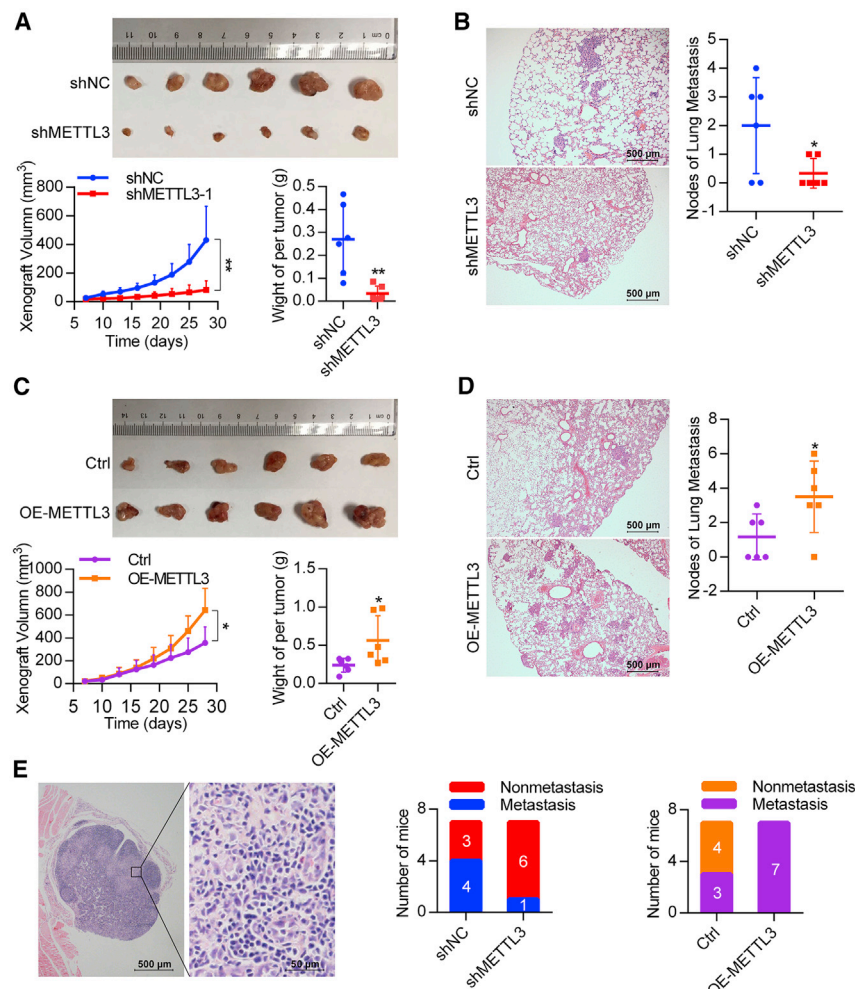
Figure 4. METTL3 Promotes OSCC Tumor Growth and Metastasis *In Vivo*

(A) Representative photograph of xenografts (upper panel); growth curves and tumor weights (lower panel) show that METTL3 knockdown significantly inhibited SCC9 xenograft growth. (B) Representative images of H&E-stained metastatic lung nodules (left) and statistical results (right) after knockdown of METTL3. (C) Representative photograph of xenografts (upper panel); growth curves and tumor weights (lower panel) after upregulation of METTL3. (D) Representative images of H&E-stained metastatic lung nodules (left) and statistical results (right) after upregulation of METTL3. (E) Representative image of H&E-stained popliteal lymph nodes (left); the proportions of mice with popliteal lymph node metastases after knockdown of METTL3 (middle); and the proportion of mice with lymph node metastases after upregulation of METTL3 (right). $*p < 0.05$, $**p < 0.01$.

mice under 4NQO treatment developed OSCC in 46.15% of the cases, while the control tongues only showed 30% OSCC formation (Figure 5N). In addition, proliferation (Ki67 expression) was increased in $Mettl3^{cKI}$ mice compared with control mice (Figure 5O). Altogether, these data suggest that $Mettl3$ KI in oral epithelial cells can augment tumor susceptibility and malignancy.

MeRIP-Seq/MeRIP-Quantitative Real-Time PCR Identified *BMI1* as a METTL3 Downstream Target

To identify the m⁶A modification targets in OSCC, we performed m⁶A MeRIP-seq using the OSCC cell line HSC3. Metagene analysis revealed that the m⁶A peaks were mainly enriched near the translation stop sites (Figure 6A). The motif AUGGAC was identified in the OSCC cell line (Figure 6B). In general, our m⁶A MeRIP-Seq data analysis results were consistent with the published m⁶A characteristics, which indicated that we successfully identified specific m⁶A sites. Gene Ontology (GO) analysis revealed that m⁶A-modified genes were abundant in regulation of RNA transcription and protein ubiquitination, chromatin modification, cell cycle, and other aspects (Figure 6C), which suggested that m⁶A may have a profound effect on OSCC. Among the m⁶A methylated genes (Table S5), visualization analysis showed that the m⁶A peaks were enriched near the stop codon of *BMI1* mRNA (Figure 6D). Moreover, MeRIP-quantitative real-time PCR assay showed that *BMI1* m⁶A modification was significantly decreased after METTL3 knockdown (Figure 6E), whereas it was increased upon METTL3 overexpression (Figure 6F), suggesting that m⁶A modification could regulate BMI1 in OSCC.

METTL3-Mediated m⁶A Modification Promoted *BMI1* mRNA Translation and Enhanced OSCC Proliferation and Metastasis

To study the molecular mechanism of *BMI1* m⁶A modification in OSCC, we first knocked down METTL3 in SCC9 cells and found

and 1.25 ± 0.7, respectively (Figure 5E). Notably, the $Mettl3^{cKO}$ mice displayed a reduced OSCC lesion area and lower histopathological grades compared with control mice (Figures 5F and 5G). In agreement, the proliferative activity determined by Ki67 IHC staining was decreased in the OSCC lesions from $Mettl3^{cKO}$ mice compared with the control mice (Figure 5H). These results show that the loss of $Mettl3$, either before or after OSCC formation, leads to inhibition of the development of malignant carcinomas in the oral region in mice.

Mettl3 Knockin (KI) Enhances Chemical Carcinogenesis in the Oral Cavity

Complementarily, $Mettl3$ was conditionally overexpressed in the oral epithelial compartment by crossing mice harboring a $Mettl3^{KI}$ allele with $K14Cre$ mice. $K14Cre;Mettl3^{KI/KI}$ ($Mettl3^{cKI}$) and $K14Cre;Mettl3^{wt/wt}$ ($Mettl3^{Ctrl}$) mice were then subjected to 4NQO treatment to induce OSCC (Figure 5J). Interestingly, our tumor incidence study revealed that the $Mettl3$ KI led to earlier OSCC appearance in mice (Figure 5K). Quantitative analysis revealed that a higher number of lesions and larger lesion areas were detected in $Mettl3^{cKI}$ mice than in the control mice (Figures 5L and 5M). The tongues of the $Mettl3^{cKI}$
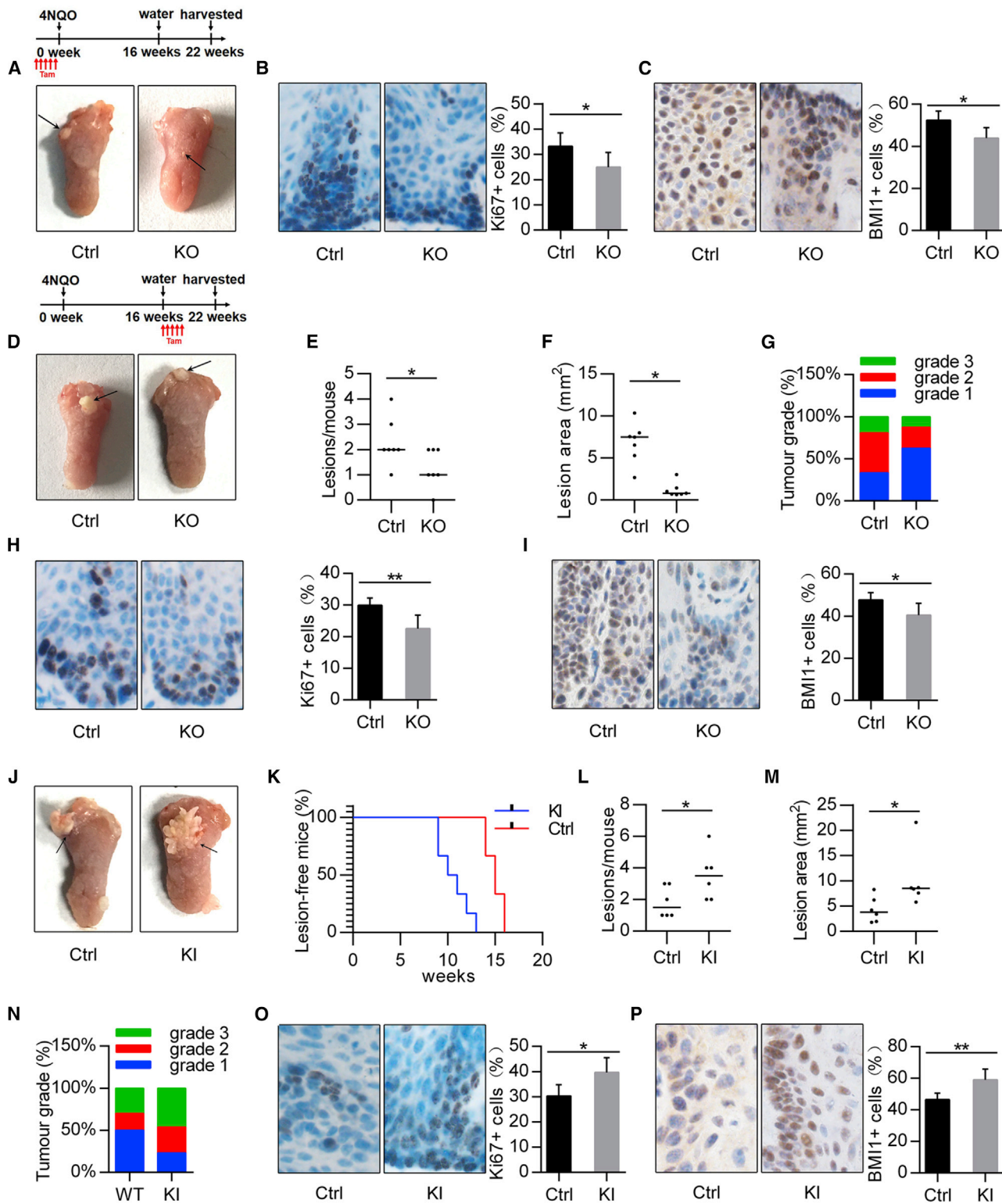
Figure 5. *Mettl3* Enhances the Chemical Carcinogenesis of the Oral Cavity

(A) Experimental design for conditional ablation of *Mettl3* in oral epithelial cells before 4NQO treatment of OSCC (top) and representative images of tongue lesions (bottom). (B and C) Immunostaining and statistical results of Ki67 (B) and BMI1 (C) in the *Mettl3^Ctrl* and *Mettl3^cKO* groups. (D) Experimental design for the conditional ablation of *Mettl3* in

(legend continued on next page)

that METTL3 knockdown reduced BMI1 protein expression without changing its mRNA level (Figures 7A and 7B), suggesting that METTL3 could regulate the BMI1 expression at the post-transcriptional level. Indeed, knockdown of METTL3 significantly reduced the proportion of *BMI1* mRNA in actively translated polysome fractions (Figure 7C), but it had little effect on its mRNA stability and protein degradation rate (Figures 7D–7F), suggesting that METTL3-mediated m6A modification is required for efficient translation of *BMI1* mRNA. At the same time, we found that overexpression of METTL3 in SCC9 cells increased BMI1 protein expression (Figure 7G) but not its mRNA level (Figure 7H). METTL3 overexpression increased the level of polysome-bound *BMI1* mRNA (Figure 7I) but did not change *BMI1* mRNA stability or protein degradation rate (Figures 7J–7L). Thus, these data reveal that METTL3-mediated m6A modification promotes *BMI1* mRNA translation in OSCC. Moreover, the expression of BMI1 was inhibited in *Mettl3cKO* OSCC compared with the control group (Figures 5C and 5I), while BMI1 expression was increased in *Mettl3cKI* mice compared with control mice (Figure 5P).

Furthermore, we co-transfected *BMI1* cDNA plasmid into METTL3 knockdown SCC9 cells and found that overexpression of BMI1 in METTL3 knockdown cells can partially reverse the function role of METTL3, including proliferation, clone formation, migration, and invasion (Figure S7).

METTL3 Recognizes m6A Residues on the *BMI1* 3′ UTR and Promoted *BMI1* Translation under the Cooperation with m6A Reader IGF2BP1

To further explore the molecular mechanisms underlying the m6A-mediated posttranscriptional regulation of *BMI1* in OSCC, we conducted luciferase reporter and mutagenesis assays. As illustrated in Figures 8A and 8B, compared with cells transfected with plasmid bearing mutant *BMI1* 3′ UTR (Mut3, Mut4), cells transfected with wild-type *BMI1* 3′ UTR substantially increased the luciferase activity, and cells co-transfected with METTL3-overexpressed plasmid also significantly increased the luciferase activity, with these data suggesting that m6A motifs of *BMI1* are essential for METTL3 to regulate BMI1 expression.

To understand how the m6A reader cooperated to promote *BMI1* translation in OSCC, SCC9 cells were transfected with different siRNA of m6A reader, including *IGF2BP1*, *IGF2BP2*, *IGF2BP3*, and *YTHDF1* siRNA. As illustrated in Figures 8C–8F, all m6A reader siRNA did not affect the expression of *BMI1* mRNA, while the expression level of BMI1 protein was significantly decreased in SCC9 cells transfected with *IGF2BP1* siRNA (Figure 8D). In addition, IGF2BP1 knockdown

decreased the BMI1 protein level in METTL3 overexpression SCC9 cells (Figure 8E). Moreover, knockdown of METTL3 and/or IGF2BP1 cooperated to decrease BMI1 protein level (Figure 8F). Taken together, our data revealed that METTL3 promotes *BMI1* translation in OSCC under the cooperation with IGF2BP1.

DISCUSSION

m6A is the most abundant modification in mRNA and is regulated by the m6A methyltransferases, demethylases, and readers. Emerging evidence has verified that the m6A modification is associated with tumorigenesis, proliferation, invasion, and metastasis and functions as an oncogene or anti-oncogene in malignant tumors. For example, METTL3 is highly expressed in gastric cancer,[27] bladder cancer,[28] colorectal carcinoma,[29] pancreatic cancer,[30] and glioblastoma,[31] and an elevated METTL3 level was found to be predictive of a poor prognosis in gastric cancer.[27] WTAP, part of the m6A mRNA methyltransferase complex, plays a similar role in most cancers, such as hepatocellular carcinoma,[32] acute myeloid leukemia,[33] diffuse large B cell lymphoma,[34] and renal cell carcinoma.[35] Moreover, the m6A reader proteins YTHDF1 and YTHDC2 are also associated with the carcinogenesis process. For example, YTHDF1 is associated with poor prognosis in liver and rectal cancer and could be an independent factor affecting the prognosis of patients.[36,37] YTHDC2 contributes to colon tumor metastasis and could potentially be used as a diagnostic marker.[38] Although the role of METTL3 has been reported in multiple cancer types, there has been no related report in OSCC. In this study, we found that RNA methylation pathway components were deregulated in OSCC. *METTL3*, *WTAP*, and *YTHDF1* were consistently expressed at a significantly higher level in OSCC tissues from TCGA dataset and our dataset. In addition, clinical data showed that OSCC tissues contained higher METTL3 levels than did adjacent normal tissues, and a higher METTL3 expression level was significantly positively associated with advanced tumor stage, advanced clinical stage, and lymph node metastasis. High METTL3 expression indicates a worse prognosis and thus can be used as a prognostic factor for OSCC patients. The potential value of the METTL3 expression level for OSCC diagnosis showed a sensitivity of 65.3% and specificity of 92%. These results suggested that METTL3 plays critical roles in OSCC development and prognosis.

Accumulating evidence supports the notion that METTL3 is involved in many biological functions in cancer cells. However, METTL3 presents a significant tumor specificity, which consequently contributes to its dual role (inhibition or promotion) in m6A modification in cancer.[25] For example, Lin et al.[39] found that deletion of METTL3 impairs liver cancer cell proliferation, migration, invasion, and epithelial-to-mesenchymal transition (EMT), while Cui et al.[19] found that knockdown of METTL3 dramatically promotes glioblastoma stem

---

oral epithelial cells after 4NQO treatment of OSCC (top) and representative images of tongue lesions (bottom). (E–G) The number of lesions (E), quantification of the lesion area (F), and tumor grades (G) were detected in the oral cavities of *Mettl3Ctrl and Mettl3cKO* mice. (H and I) Immunostaining and statistical results of Ki67 (H) and BMI1 (I) staining in *Mettl3Ctrl and Mettl3cKO* groups. (J) Representative images of tongue lesions 16 weeks after 4NQO treatment. (K) Statistical results of tumor incidence in *Mettl3cKI and Mettl3Ctrl* mice. (L and M) Quantitation of lesion numbers (L) and lesion areas (M) visible in the control and *Mettl3* knockin groups. (N) Quantification of tumor grades in the *Mettl3cKI and Mettl3Ctrl* groups. (O and P) Immunostaining and statistical results for Ki67 (O) and BMI1 (P) in *Mettl3cKI and Mettl3Ctrl* groups. KO, *K14CreER;Mettl3fl/fl* (*Mettl3cKO*); Ctrl, *K14CreER;Mettl3wt/wt* (*Mettl3Ctrl*); KI, *K14Cre;Mettl3KI/KI* (*Mettl3cKI*); Ctrl, *K14Cre;Mettl3wt/wt* (*Mettl3Ctrl*). The arrow indicates an OSCC lesion.
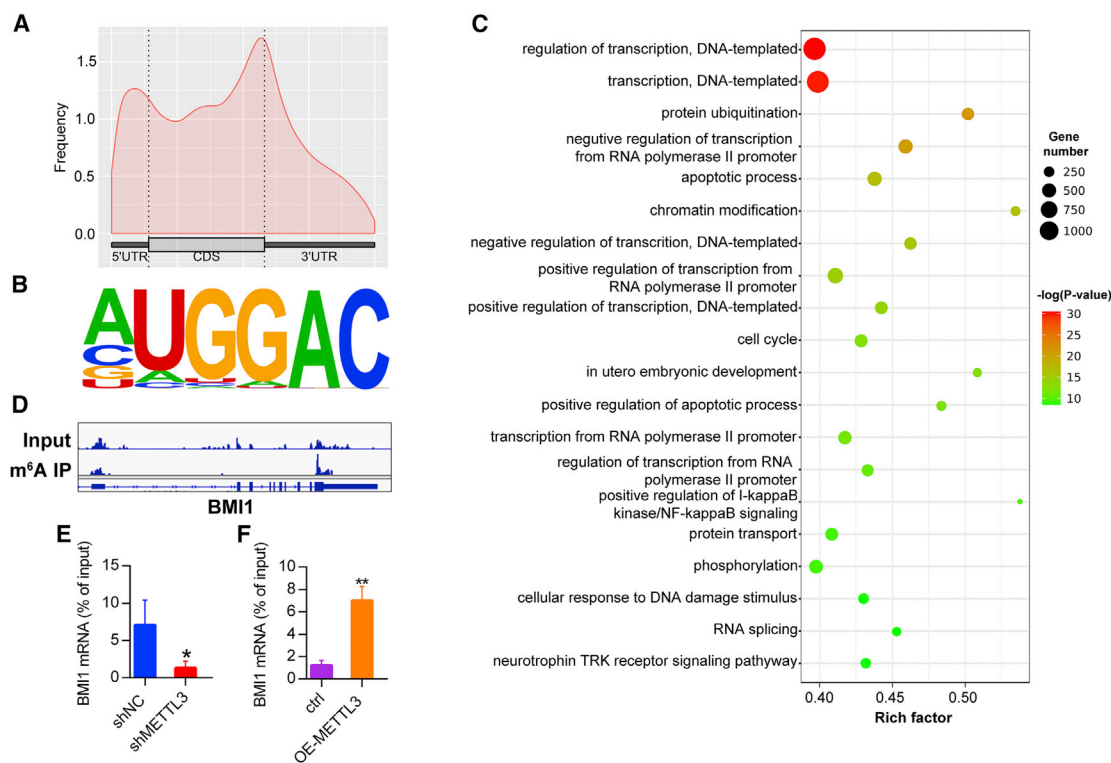
Figure 6. MeRIP-Seq/MeRIP-Quantitative Real-Time PCR Identifies *BMI1* as a Downstream Target of METTL3-Mediated m⁶A Modification

(A) Metagene profiles of m⁶A distribution across the transcriptome in OSCC cell line HSC3. (B) Consensus sequence motif for m⁶A methylation identified in OSCC cells. (C) Gene ontology and enrichment analysis of m⁶A-modified genes. (D) Representative m⁶A modification of *BMI1* in OSCC. (E) *BMI1* m⁶A modification was significantly decreased after METTL3 knockdown in SCC9 cells. (F) *BMI1* m⁶A modification was significantly increased after METTL3 overexpression in SCC9 cells.

cell growth, self-renewal, and tumorigenesis. METTL3 also plays an important role in stem cell self-renewal and maintenance,[40] cell cycle arrest, and differentiation and autophagy.[41,42] In this study, we demonstrated that OSCC cells, especially cells with high metastatic potential, showed enhanced METTL3 expression and that overexpression of METTL3 in OSCC cells promoted OSCC self-renewal, proliferation, migration, and invasion *in vitro*. In contrast, knockdown of METTL3 resulted in decreased OSCC cell self-renewal, proliferation, migration, and invasion *in vitro*.

To date, *in vivo* studies have demonstrated that METTL3 is associated with tumorigenesis and lung metastasis in liver cancer,[16] colorectal carcinoma,[29] gastric cancer,[27] bladder cancer,[28] and glioblastoma.[19] However, reports on METTL3 and lymph node metastasis *in vivo* are rare. In this study, we established subcutaneous xenograft tumor, lung metastasis, and lymph node metastasis models in nude mice and found that METTL3 contributed to OSCC tumorigenesis and the formation of metastatic foci. Overexpression of METTL3 effectively promoted subcutaneous tumor growth in nude mice and significantly promoted lung and popliteal lymph node metastasis compared with the control groups, while knockdown of METTL3 inhibited subcutaneous tumor growth and the incidence of pulmonary and popliteal lymph node metastasis. Thus, these data revealed a functional role of METTL3 in promoting OSCC tumorigenesis and metastasis *in vivo*.

In this study, we also combined a genetically modified mouse model to delete or overexpress *Mettl3* in the oral mucosa followed by a protocol of chemical-induced carcinogenesis with 4NQO, which allowed us to dissect the role of Mettl3 at different steps in OSCC initiation and progression. The 4NQO model of oral carcinogenesis generates progressive changes in the murine oral mucosa that eventually lead to OSCC. In this mouse model, ablation of *Mettl3* before carcinogen treatment resulted in suppression of OSCC initiation. In addition, mice with depletion of *Mettl3* after OSCC formation developed fewer dysplastic lesions and carcinomas *in situ*, demonstrating that Mettl3 is necessary for OSCC progression. Although the role of METTL3 has been characterized in multiple cancer lines, this is the first report to provide functional evidence that Mettl3 is required for cancer development in a genetic mouse model. The observation of accelerated OSCC formation in *Mettl3* overexpression mice suggests that Mettl3 might serve as a relevant oncogenic component for tongue epithelium and reinforces the notion that mRNA posttranslational modification has a decisive role in malignancy development.

METTL3-mediated m⁶A modification regulates all phases of the mRNA life cycle, including RNA splicing, nuclear export, translation, and degradation.[16,20,43] In the present study, METTL3 protein level was found to be positively correlated with m⁶A methylation level in OSCC tissues. Our m⁶A MeRIP-seq and MeRIP-quantitative real-time PCR results also demonstrated that a subset of important
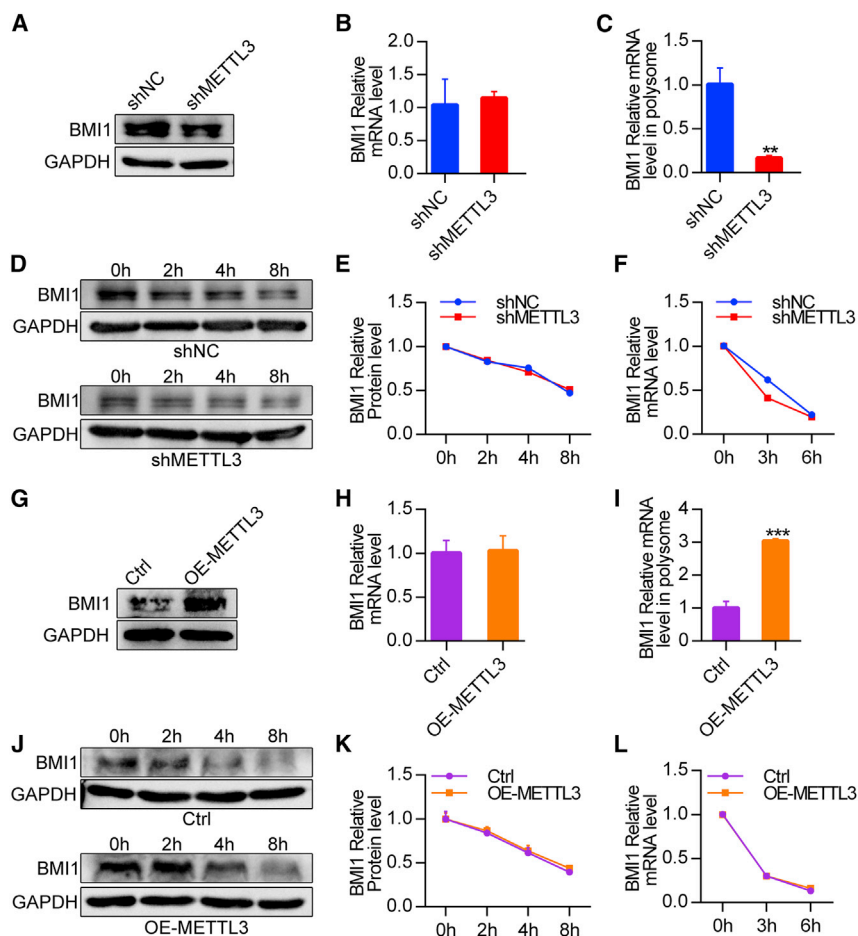
Figure 7. METTL3 Promotes *BMI1* mRNA m⁶A Modification and Translation

(A) The expression of BMI1 protein was downregulated after METTL3 knockdown in SCC9 cells. (B) The expression of *BMI1* mRNA remained unchanged after METTL3 knockdown in SCC9 cells. (C) Polysome-fractionated samples analyzed by quantitative real-time PCR showed that polysome-bound *BMI1* mRNA levels were significantly decreased after METTL3 knockdown in SCC9 cells. (D–F) Protein and RNA stability assays showed that the degradation rate of *BMI1* mRNA (F) and protein (D, the results of western blot) and E, the statistical results) was not different between control shRNA and METTL3 knockdown SCC9 cells. (G) The expression of BMI1 protein was upregulated after METTL3 overexpression in SCC9 cells. (H) The expression of *BMI1* mRNA remained unchanged after METTL3 overexpression in SCC9 cells. (I) Polysome-bound *BMI1* mRNA levels were significantly increased in METTL3-overexpressing SCC9 cells. (J–L) The degradation rate of *BMI1* mRNA (L) and protein (J, the results of western blot) and K, the statistical results) was not different between control cDNA and METTL3-overexpressing SCC9 cells.

oncogenes was selectively m⁶A modified in OSCC, including the OSCC oncogene *BMI1*, a cancer stem cell marker that plays an important role in the progression and prognosis of OSCC and promotes chemoresistance and metastasis in head and neck squamous cell carcinoma in our previous research.[44] We further found that depletion of METTL3 decreased the BMI1 protein level but had little effect on its mRNA level, mRNA stability, and protein degradation rate, suggesting that METTL3 could regulate *BMI1* mRNA translation. Indeed, the polysome-bound *BMI1* mRNA level was significantly decreased when METTL3 was depleted. Moreover, METTL3 was found to recognize m⁶A residues on the *BMI1* 3′ UTR and promoted *BMI1* translation under the cooperation with m⁶A reader IGF2BP1. Thus, these data indicate that METTL3 catalyzes the m⁶A modification on *BMI1* mRNA and promotes its translation rather than degradation in OSCC.

MATERIALS AND METHODS
Clinical Samples
Two clinical patient cohorts were used in this study: (1) a training sample set: 101 OSCC tissue samples and 50 normal oral mucosal tissue samples (collected from June 2004 to September 2014); and (2) a validation sample set (tissue chip): 50 OSCC tissue samples and 27

corresponding adjacent noncancerous tissue samples (collected from November 2016 to April 2019). All of the samples were collected at the Department of Oral and Maxillofacial Surgery, First Affiliated Hospital, Sun Yat-Sen University. None of the patients had undergone preoperative radiation or chemotherapy, and all samples were obtained with informed consent and their use was approved by the Institutional Review Board of the First Affiliated Hospital of Sun Yat-Sen University. The clinical characteristics of the samples are summarized in Table S6. Survival of the patients in the training sample set was calculated from the day of diagnosis to the date of the latest follow-up (or death). The median duration of follow-up was 22 months (range, 3–106 months).

Moreover, seven pairs of OSCC and adjacent normal oral mucosa tissues (Table S6) were used to detect the expression of the m⁶A methylation modification enzyme by quantitative real-time PCR.

IHC Staining
Tissue slides were routinely deparaffinized and rehydrated, followed by antigen retrieval. Then, the slides were treated with 3% H_2O_2 and separately incubated with antibody targeting METTL3 (1:500, Abcam), Ki67 (1:200, Abcam), and BMI1 (1:200, Affinity) overnight at 4°C. After washing, the slides were stained using a diaminobenzidine (DAB) detection kit (Gene Tech, China) and counterstained with hematoxylin. For METTL3, each sample was scored according to the proportion of positively stained cells (proportion score, 0–4) and the staining intensity (intensity score, 0–3). The staining index was calculated by multiplying the proportion score and the intensity score. The cutoff value for the IHC score was chosen according to the
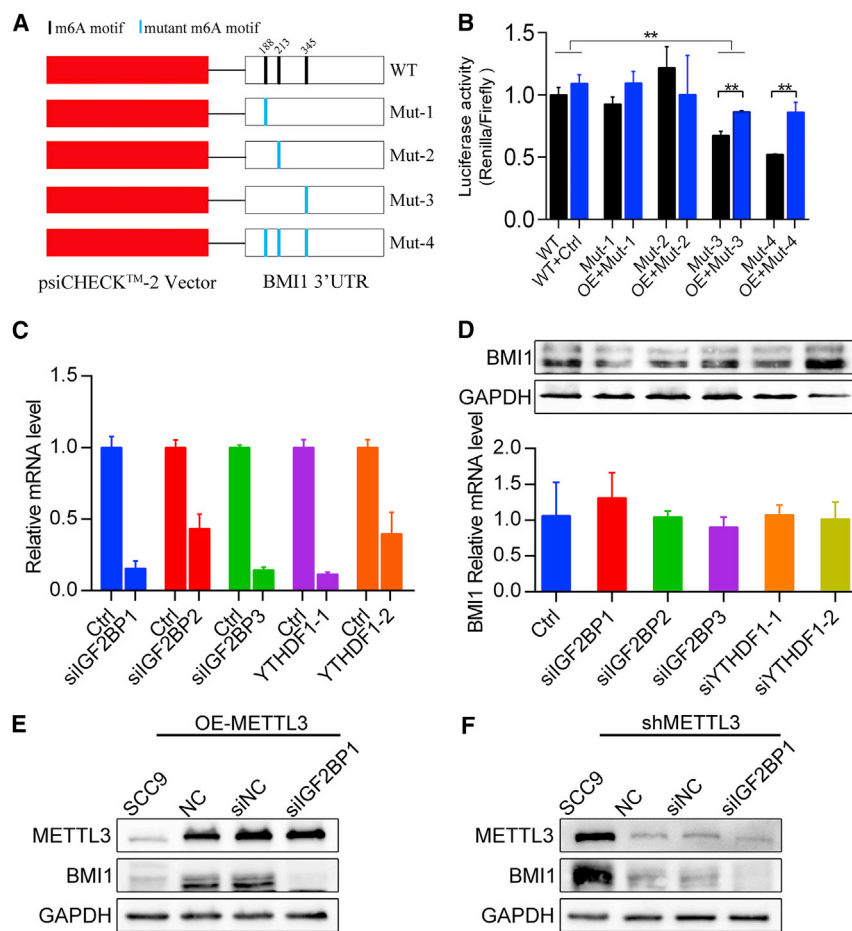
Figure 8. METTL3 Recognizes m⁶A Residues on the *BMI1* 3′ UTR and Promoted *BMI1* Translation under the Cooperation with m⁶A Reader IGF2BP1

(A) Luciferase reporter constructs containing human *BMI1* 3′ UTR that have m⁶A motifs or mutant (A-to-G mutation) m⁶A sites (Mut1, Mut2, Mut3, Mut4) are shown. (B) Relative luciferase activities of SCC9 cells co-transfected with plasmids containing wild-type or mutant *BMI1* 3′ UTR and *METTL3* cDNA. Renilla luciferase activities were measured and normalized to firefly luciferase activity. (C) The mRNA level of m⁶A readers in SCC9 cells treated with control or siRNAs. (D) Western blotting (up) and quantitative real-time PCR (down) results of BMI1 expression in SCC9 cells treated with control or *IGF2BP1*, *IGF2BP2*, *IGF2BP3*, and *YTHDF1* siRNAs. (E) The BMI1 protein expression in METTL3 overexpressed cells treated with control or *IGF2BP1* siRNAs. (F) The BMI1 protein expression in METTL3 knockdown cells treated with control or *IGF2BP1* siRNAs.

Youden index to define low and high METTL3 expression. For Ki67 and BMI1, the proportion of positively stained cells was calculated.

Cell Culture and Transfection

The HSC3 cell line was purchased from the cell bank of the Japanese Collection of Research Bioresource (JCRB). SCC9, SCC15, SCC25 were purchased from the ATCC. HOK cells were purchased from ScienCell, and UM1 was provided by Xiaofeng Zhou.

SCC9, SCC15, SCC25, and UM1 cells were cultured in DMEM/F12 supplemented with 10% fetal bovine serum (FBS) and 1% penicillin-streptomycin. HOK cells were cultured with RPMI 1640 medium containing 15% FBS and 1% antibiotics. All of the cells were grown in a 5% CO₂ incubator at 37°C. siRNA of m⁶A reader was purchased from OBiOc (Shanghai, China) and transfected into SCC9 cells following the manufacturer's instructions. The siRNA sequences of *IGF2BP1*, *IGF2BP2*, *IGF2BP3*, and *YTHDF1* are listed in Table S7.

Lentivirus vectors containing *METTL3* cDNA or shRNA were purchased from OBiOc (Shanghai, China). In brief, to construct a lentivirus-mediated silencing vector, three shRNA sequences targeting human *METTL3* were cloned into a pLKD-CMV-G&PR-U6-shRNA vector, and the sequence with the best knockdown effect (shRNA1) was chosen for further study (Figure S8). The indicated three shRNA sequences are listed in Table S8. For METTL3 overexpression, the full-length cDNA sequences of human *METTL3* (gene ID: 019852) were cloned into a pLenti-EF1a-EGFP-P2A-Puro-CMV-MCS-3Flag lentivirus vector, and the primer sequences for the cloning of *METTL3* cDNA are as follows: forward, 5′-GTTTAGTGAACCGTCAGATCGAATTCGC CACCATGTC-3′, reverse, 5′-TCATCGTCATCC TTGTAGTCGAATTCTAAATTCTTAGGTTTA GAGAT-3′. For knockdown or overexpression of METTL3, SCC9 cells were infected with lentivirus with 5 μg/mL Polybrene, and after 48 h, 2 μg/mL puromycin was added to the culture medium to select the infected cells.

Western Blotting

Total cellular protein was harvested by lysing cells with radioimmunoprecipitation assay (RIPA) lysis buffer supplemented with proteinase inhibitor cocktail. Aliquots (20 μg) of cellular proteins were resolved via SDS-PAGE (10%), electrotransferred onto polyvinylidene fluoride (PVDF) membranes, and immunoprobed. Then, the protein antibody complexes were detected with enhanced chemiluminescence (ECL) detection reagents. Primary antibodies against the following targets were used: METTL3 (1:1,000, Abcam) and BMI1 (1:1,000, Abcam). GAPDH (1:1,000, Abcam) was used as an internal control.

Quantitative Real-Time PCR

Total RNA was isolated using TRIzol (Invitrogen, USA) reagent following the manufacturer's instructions, and cDNA was synthesized using a PrimeScript RT master mix kit (TaKaRa, Japan). Then, quantitative real-time PCR was performed using a TB Green

Premix Ex Taq II kit (TaKaRa, Japan) on a Bio-Rad CXF96 real-time system (Bio-Rad, USA). β-Actin served as the internal control, and the relative expression levels of mRNA were assessed through the comparative threshold cycle method ($2^{-\Delta\Delta Ct}$). All primers used in this study are listed in Table S9.

Cell Proliferation Assay and Colony Formation Assays

Cell proliferation was measured using Cell Counting Kit-8 (CCK-8) (Dojindo, Japan) following the manufacturer's protocol. In brief, cells were plated at 3×10^3 cells per well in 96-well plates and cultured at 37°C for 24, 48, 72, and 96 h. Then, 10 μL of CCK-8 solution was added into the cell culture medium. After 2 h, the absorbance at 450 nm was recorded using a microplate reader (Thermo Fisher Scientific, USA).

In the colony formation experiments, the cells were plated into six-well plates at a density of 200 cells/mL in triplicate and cultured for 14 days, after which the colonies were fixed with 4% formaldehyde for 15 min and stained with 0.1% crystal violet for 10 min. Then, the colonies were photographed, and colonies larger than 1 mm (>50 cells/clone) were counted.

Cell Migration and Invasion Assay

Cell migration and invasion assays were performed using BD BioCoat control cell culture inserts (BD Biosciences, USA) and Matrigel invasion chambers (BD Biosciences, USA), respectively. In brief, cells (5 × 10^4 cells/well) suspended in FBS-free DMEM/F12 culture medium were added into the upper chamber, and 1 mL of DMEM/F12 containing 10% FBS was added to the lower compartment. After incubation for 24 h, the cells that remained on the upper surface of the filter membrane were wiped off, and the cells that had crossed the filter membrane and adhered on the lower membrane surface were stained with 0.1% crystal violet. Images of the stained lower surface were captured, and the cells were quantified under a microscope in five random fields.

Sphere Formation Assays

Cells were planted on ultralow attachment six-well plates at a density of 3,000 cells per well and cultured in serum-free DMEM/F12 culture medium supplemented with 1× B27 supplement, 20 ng/mL human recombinant epidermal growth factor (Sigma, USA), and 20 ng/mL basic fibroblast growth factor (Sigma, USA). The medium was replenished with fresh medium every 3 days. After 2 weeks, images of the spheres were captured using a microscope, and clones with a diameter of more than 50 μm were counted.

m⁶A MeRIP-Seq and MeRIP-Quantitative Real-Time PCR

MeRIP-seq and MeRIP-quantitative real-time PCR were performed according to the published procedure with slight modifications.[45] Briefly, total RNA was fragmented into 100-nt RNA fragments using $ZnCl_2$ and incubated with anti-m⁶A polyclonal antibody (Synaptic Systems, 202003) for 2 h at 4°C and then with protein A/G magnetic beads (Thermo Fisher Scientific, 88802) at 4°C for an additional 2 h to obtain immunoprecipitated RNA fragments. The bound RNA was

eluted from the beads with m⁶A (ApexBio Technology, B5993) in immunoprecipitation (IP) buffer, and RNA concentration was measured with a Qubit RNA HS assay kit (Invitrogen, Q32852). The purified RNA was used for RNA-seq library construction and quantitative real-time PCR, and the primers used in the MeRIP-quantitative real-time PCR are listed in Table S9. The RNA-seq library was constructed with a NEBNext Ultra RNA library prep kit (NEB, E6177). Both the input sample without IP and the m⁶A IP samples were subjected to 75-bp, single-end sequencing on an Illumina Next-Seq 500 sequencer. After 3′ adaptor trimming and removal of inferior quality reads by Cutadapt software (v1.9.3), clean reads of all the libraries were aligned to the reference genome (UCSC HG38) using Hisat2 software (v2.0.4). Methylated sites on RNAs (peaks) were identified with MACS software. GO and Pathway enrichment analyses of the differentially methylated protein coding genes were conducted.

Protein and RNA Stability Assays

To measure protein stability, lentivirus-infected SCC9 cells were treated with cycloheximide (CHX, 100 μg/mL) at 0, 2, 4, and 8 h, and the expression of BMI1 was measured via western blotting and normalized to GAPDH expression. To measure RNA stability, we treated the lentivirus-infected SCC9 cells with actinomycin D (ActD, 5 μg/mL) for 0, 3, and 6 h. Total RNA was then isolated and analyzed via quantitative real-time PCR, and the relative level of *BMI1* was quantified and normalized to *β-actin*.

Ribosome-Nascent Chain Complex (RNC) Extraction

To investigate the translation ability of *BMI1* mRNA, an RNC-quantitative real-time PCR assay was used. The RNC was extracted using sucrose gradient centrifugation as described by Esposito et al.,[46] with certain modifications. In brief, the cells were treated with 100 μg/mL cycloheximide for 15 min and lysed in cell lysis buffer (1% Triton X-100 in ribosome buffer [RB buffer] containing 20 mM HEPES-KOH [pH 7.4], 15 mM $MgCl_2$, 200 mM KCl, 100 μg/mL cycloheximide, and 2 mM dithiothreitol) for 30 min in an ice bath. The nuclei and cell debris were removed by centrifugation at $16,200 \times g$ for 10 min at 4°C, and the supernatants were collected and transferred to the top of 20 mL of 30% sucrose buffer. Finally, the RNCs were pelleted by ultracentrifugation at $185,000 \times g$ for 5 h at 4°C, and RNA in the polysome fraction was extracted, reverse transcribed, and subjected to quantitative real-time PCR according to the above methods.

RNA m⁶A Dot Blot Assays

2 μg of total RNA extracted from the OSCC and para-carcinoma tissues were denatured at 95°C for 3 min and crosslinked to the Hybond-N+ membrane in a crosslinker twice using 1,200 μJ for 50 s. The membrane was analyzing using m⁶A antibody (Synaptic Systems, 202003), and the intensity of dot blot signal was quantified by ImageJ.

Dual-Luciferase Reporter Assay

Plasmids containing wild-type *BMI1* 3′ UTR, mutant *BMI1* 3′ UTR (mutated A of the m⁶A sites with G), or *METTL3* cDNA were constructed. Four plasmids containing *BMI1* mutant were

constructed (Mut1–Mut4). Cells were co-transfected with plasmids containing wild-type or mutant *BMI1* 3′ UTR and *METTL3* cDNA using Lipofectamine 3000 according to the manufacturer's protocol. At 24 h after transfection, firefly and Renilla luciferase activities were measured consecutively by using a dual-luciferase reporter assay system. Finally, ratios of luminescence from Renilla to firefly luciferase were calculated.

Tumorigenesis and Metastasis Assay *In Vivo*

Female BALB/c nude mice (4-week-old) were purchased from Model Animal Research Center (Nanjing, China). SCC9 cells stably infected with lentivirus containing *METTL3*-targeting shRNAs and *METTL3* cDNA were used to investigate the effect of METTL3 on OSCC tumor growth and metastasis *in vivo*. To construct the subcutaneous tumorigenesis model, the cells were suspended in 100 μL of PBS and Matrigel matrix (BD Biosciences, USA) (1:1) and injected into the right flanks of 6-week-old female BALB/c nude mice. The xenografts were measured by with a Vernier caliper every 3 days from 1 week after inoculation, and the tumor volumes were calculated using the following formula: volume = (length $\times$ width2)/2. The mice were euthanized before the tumor volumes reached 1,000 mm^3, and the tumors were weighed. For the lung metastasis assay, 2×10^6/ 0.1 mL stably infected SCC9 cells were injected into the tail vein of BALB/c nude mice. After 6 weeks, the mice were sacrificed, and the lungs were embedded, sectioned, and stained with H&E to calculate the number of metastatic nodules. The image of lung tissues (Figure S9) to count the number of metastatic nodules were jigsaw combined all the sections of lung together through porta pulmonis as in our previous report.[47]

To construct the lymph node metastasis model, we injected 1×10^5/ 50 μL stably infected SCC9 cells into the left hind footpads of BALB/c mice. After 6 weeks, the mice were euthanized, and the popliteal lymph nodes of the left hind limbs were counted and analyzed through H&E staining.

Mettl3 KO or KI in a 4NQO-Induced OSCC Model

K14Cre and *K14CreER* mice were purchased from The Jackson Laboratory. *Mettl3$^{fl/fl}$*, *Mettl3$^{KI/KI}$* mice were kindly provided by Prof. Quan Yuan from the West China Hospital of Stomatology. Mouse colonies were maintained in a certified animal facility. The mouse experiments performed were approved by the Laboratory Animal Center of Sun Yat-Sen University.

Mice were treated with 100 μg/mL 4NQO in drinking water as previously described.[44] For the Mettl3 KO study, male and female *K14CreER*;*Mettl3$^{wt/fl}$* mice were used as breeders for generation of *K14CreER*;*Mettl3$^{wt/wt}$* (*Mettl3^{Ctrl}*) and *K14CreER*;*Mettl3$^{fl/fl}$* (*Mettl3^{cKO}*) mice. *Mettl3^{cKO}* and *Mettl3^{Ctrl}* mice were injected with tamoxifen (1 mg per mouse per day) for 5 consecutive days before 4NQO application (prevention model) or 16 weeks after 4NQO application (treatment model). For the Mettl3 overexpression study, we crossed male and female *K14Cre*;*Mettl3$^{KI/wt}$* mice to obtain *K14Cre*; *Mettl3$^{wt/wt}$* (*Mettl3^{Ctrl}*) and *K14Cre*;*Mettl3$^{KI/KI}$* (*Mettl3^{cKI}*) mice.

Mice were treated with 4NQO at 6–8 weeks of age. The expression level of *Mettl3* was confirmed by PCR in *Mettl3* KO and KI mice after tamoxifen induction (Figure S10).

Statistical Analysis

The data are presented as the mean ± standard deviation (SD). Statistical analyses were carried out using SPSS 17.0 software. Unpaired two-tailed Student's t tests were applied to compare data between two groups, and one-way ANOVA was used for multiple comparisons. A chi-square test was used to evaluate the statistical significance of differences in IHC scores between OSCC and adjacent noncancerous samples. Survival analysis was performed with a Kaplan-Meier curve and log rank test. Values of p less than 0.05 were considered statistically significant.

Study Approval

Genetically modified mouse experiments performed were approved by the Laboratory Animal Center of Sun Yat-Sen University (SYSU-IACUC-2019-000077). Subcutaneous xenografted tumor, lung metastasis, and lymph node metastasis animal experiments were approved by the Ethics Committee of the Cancer Center of Sun Yat-Sen University (L102012018090B). All samples were obtained with informed consent and the use was approved by the Institutional Review Board of the First Affiliated Hospital of Sun Yat-Sen University (2016074).

SUPPLEMENTAL INFORMATION

Supplemental Information can be found online at https://doi.org/10.1016/j.ymthe.2020.06.024.

AUTHORS CONTRIBUTIONS

A.W. and D.C. conceived of, designed, and supervised the study; L.L., Y.W., Q.L., J.L., J.C., and M.C. performed the experiments and analyzed the data; Q.H., L.Z., Z.H., J.C., L.P., H.R., and F.G. provided technical assistance with the experiments; L.L. wrote the manuscript. All co-authors have reviewed and approved this version of the manuscript.

CONFLICTS OF INTEREST

The authors declare no competing interests.

REFERENCES

1. Hedberg, M.L., Goh, G., Chiosea, S.I., Bauman, J.E., Freilino, M.L., Zeng, Y., Wang, L., Diergaarde, B.B., Gooding, W.E., Lui, V.W., et al. (2016). Genetic landscape of

metastatic and recurrent head and neck squamous cell carcinoma. J. Clin. Invest. *126*, 169–180.

2. Ferlay, J., Shin, H.R., Bray, F., Forman, D., Mathers, C., and Parkin, D.M. (2010). Estimates of worldwide burden of cancer in 2008: GLOBOCAN 2008. Int. J. Cancer *127*, 2893–2917.

3. Leemans, C.R., Braakhuis, B.J., and Brakenhoff, R.H. (2011). The molecular biology of head and neck cancer. Nat. Rev. Cancer *11*, 9–22.

4. Jithesh, P.V., Risk, J.M., Schache, A.G., Dhanda, J., Lane, B., Liloglou, T., and Shaw, R.J. (2013). The epigenetic landscape of oral squamous cell carcinoma. Br. J. Cancer *108*, 370–379.

5. Bavle, R.M., Venugopal, R., Konda, P., Muniswamappa, S., and Makarla, S. (2016). Molecular classification of oral squamous cell carcinoma. J. Clin. Diagn. Res. *10*, ZE18–ZE21.

6. González-Ramírez, I., Soto-Reyes, E., Sánchez-Pérez, Y., Herrera, L.A., and García-Cuellar, C. (2014). Histones and long non-coding RNAs: the new insights of epigenetic deregulation involved in oral cancer. Oral Oncol. *50*, 691–695.

7. Roundtree, I.A., Evans, M.E., Pan, T., and He, C. (2017). Dynamic RNA modifications in gene expression regulation. Cell *169*, 1187–1200.

8. Liu, J., Yue, Y., Han, D., Wang, X., Fu, Y., Zhang, L., Jia, G., Yu, M., Lu, Z., Deng, X., et al. (2014). A METTL3-METTL14 complex mediates mammalian nuclear RNA N^6-adenosine methylation. Nat. Chem. Biol. *10*, 93–95.

9. Ping, X.L., Sun, B.F., Wang, L., Xiao, W., Yang, X., Wang, W.J., Adhikari, S., Shi, Y., Lv, Y., Chen, Y.S., et al. (2014). Mammalian WTAP is a regulatory subunit of the RNA N6-methyladenosine methyltransferase. Cell Res. *24*, 177–189.

10. Zheng, G., Dahl, J.A., Niu, Y., Fedorcsak, P., Huang, C.M., Li, C.J., Vågbø, C.B., Shi, Y., Wang, W.L., Song, S.H., et al. (2013). ALKBH5 is a mammalian RNA demethylase that impacts RNA metabolism and mouse fertility. Mol. Cell *49*, 18–29.

11. Jia, G., Fu, Y., Zhao, X., Dai, Q., Zheng, G., Yang, Y., Yi, C., Lindahl, T., Pan, T., Yang, Y.G., and He, C. (2011). N^6-methyladenosine in nuclear RNA is a major substrate of the obesity-associated FTO. Nat. Chem. Biol. *7*, 885–887.

12. Wang, X., Zhao, B.S., Roundtree, I.A., Lu, Z., Han, D., Ma, H., Weng, X., Chen, K., Shi, H., and He, C. (2015). N^6-methyladenosine modulates messenger RNA translation efficiency. Cell *161*, 1388–1399.

13. Huang, H., Weng, H., Sun, W., Qin, X., Shi, H., Wu, H., Zhao, B.S., Mesquita, A., Liu, C., Yuan, C.L., et al. (2018). Recognition of RNA N^6-methyladenosine by IGF2BP proteins enhances mRNA stability and translation. Nat. Cell Biol. *20*, 285–295.

14. Meyer, K.D., Patil, D.P., Zhou, J., Zinoviev, A., Skabkin, M.A., Elemento, O., Pestova, T.V., Qian, S.-B., and Jaffrey, S.R. (2015). 5′ UTR m⁶A promotes cap-independent translation *163*, 999–1010.

15. Geula, S., Moshitch-Moshkovitz, S., Dominissini, D., Mansour, A.A., Kol, N., Salmon-Divon, M., Hershkovitz, V., Peer, E., Mor, N., Manor, Y.S., et al. (2015). Stem cells. m6A mRNA methylation facilitates resolution of naïve pluripotency toward differentiation. Science *347*, 1002–1006.

16. Fustin, J.M., Doi, M., Yamaguchi, Y., Hida, H., Nishimura, S., Yoshida, M., Isagawa, T., Morioka, M.S., Kakeya, H., Manabe, I., and Okamura, H. (2013). RNA-methylation-dependent RNA processing controls the speed of the circadian clock. Cell *155*, 793–806.

17. Lin, Z., Hsu, P.J., Xing, X., Fang, J., Lu, Z., Zou, Q., Zhang, K.J., Zhang, X., Zhou, Y., Zhang, T., et al. (2017). Mettl3-/Mettl14-mediated mRNA N^6-methyladenosine modulates murine spermatogenesis. Cell Res. *27*, 1216–1230.

18. Yoon, K.J., Ringeling, F.R., Vissers, C., Jacob, F., Pokrass, M., Jimenez-Cyrus, D., Su, Y., Kim, N.S., Zhu, Y., Zheng, L., et al. (2017). Temporal control of mammalian cortical neurogenesis by m⁶A methylation. Cell *171*, 877–889.e17.

19. Cui, Q., Shi, H., Ye, P., Li, L., Qu, Q., Sun, G., Sun, G., Lu, Z., Huang, Y., Yang, C.G., et al. (2017). m⁶A RNA methylation regulates the self-renewal and tumorigenesis of glioblastoma stem cells. Cell Rep. *18*, 2622–2634.

20. Lin, S., Choe, J., Du, P., Triboulet, R., and Gregory, R.I. (2016). The m⁶A methyltransferase METTL3 promotes translation in human cancer cells. Mol. Cell *62*, 335–345.

21. Cai, X., Wang, X., Cao, C., Gao, Y., Zhang, S., Yang, Z., Liu, Y., Zhang, X., Zhang, W., and Ye, L. (2018). HBXIP-elevated methyltransferase METTL3 promotes the progression of breast cancer via inhibiting tumor suppressor let-7g. Cancer Lett. *415*, 11–19.

22. Chen, M., Wei, L., Law, C.T., Tsang, F.H., Shen, J., Cheng, C.L., Tsang, L.H., Ho, D.W., Chiu, D.K., Lee, J.M., et al. (2018). RNA N6-methyladenosine methyltransferase-like 3 promotes liver cancer progression through YTHDF2-dependent posttranscriptional silencing of SOCS2. Hepatology *67*, 2254–2270.

23. Li, Z., Weng, H., Su, R., Weng, X., Zuo, Z., Li, C., Huang, H., Nachtergaele, S., Dong, L., Hu, C., et al. (2017). FTO plays an oncogenic role in acute myeloid leukemia as a N^6-methyladenosine RNA demethylase. Cancer Cell *31*, 127–141.

24. Wang, S., Chai, P., Jia, R., and Jia, R. (2018). Novel insights on m6A RNA methylation in tumorigenesis: a double-edged sword. Mol. Cancer *17*, 101.

25. He, L., Li, J., Wang, X., Ying, Y., Xie, H., Yan, H., Zheng, X., and Xie, L. (2018). The dual role of N6-methyladenosine modification of RNAs is involved in human cancers. J. Cell. Mol. Med. *22*, 4630–4639.

26. Wang, W., Liu, Z., Zhao, L., Sun, J., He, Q., Yan, W., Lu, Z., and Wang, A. (2017). Hexokinase 2 enhances the metastatic potential of tongue squamous cell carcinoma via the SOD2-H2O2 pathway. Oncotarget *8*, 3344–3354.

27. Yue, B., Song, C., Yang, L., Cui, R., Cheng, X., Zhang, Z., and Zhao, G. (2019). METTL3-mediated N6-methyladenosine modification is critical for epithelial-mesenchymal transition and metastasis of gastric cancer. Mol. Cancer *18*, 142.

28. Han, J., Wang, J.Z., Yang, X., Yu, H., Zhou, R., Lu, H.C., Yuan, W.B., Lu, J.C., Zhou, Z.J., Lu, Q., et al. (2019). METTL3 promote tumor proliferation of bladder cancer by accelerating pri-miR221/222 maturation in m6A-dependent manner. Mol. Cancer *18*, 110.

29. Li, T., Hu, P.S., Zuo, Z., Lin, J.F., Li, X., Wu, Q.N., Chen, Z.H., Zeng, Z.L., Wang, F., Zheng, J., et al. (2019). METTL3 facilitates tumor progression via an m6A-IGF2BP2-dependent mechanism in colorectal carcinoma. Mol. Cancer *18*, 112.

30. Xia, T., Wu, X., Cao, M., Zhang, P., Shi, G., Zhang, J., Lu, Z., Wu, P., Cai, B., Miao, Y., and Jiang, K. (2019). The RNA m6A methyltransferase METTL3 promotes pancreatic cancer cell proliferation and invasion. Pathol. Res. Pract. *215*, 152666.

31. Li, F., Yi, Y., Miao, Y., Long, W., Long, T., Chen, S., Cheng, W., Zou, C., Zheng, Y., Wu, X., et al. (2019). N^6-methyladenosine modulates nonsense-mediated mRNA decay in human glioblastoma. Cancer Res. *79*, 5785–5798.

32. Chen, Y., Peng, C., Chen, J., Chen, D., Yang, B., He, B., Hu, W., Zhang, Y., Liu, H., Dai, L., et al. (2019). WTAP facilitates progression of hepatocellular carcinoma via m6A-HuR-dependent epigenetic silencing of ETS1. Mol. Cancer *18*, 127.

33. Bansal, H., Yihua, Q., Iyer, S.P., Ganapathy, S., Proia, D.A., Penalva, L.O., Uren, P.J., Suresh, U., Carew, J.S., Karnad, A.B., et al. (2014). WTAP is a novel oncogenic protein in acute myeloid leukemia. Leukemia *28*, 1171–1174.

34. Kuai, Y., Gong, X., Ding, L., Li, F., Lei, L., Gong, Y., Liu, Q., Tan, H., Zhang, X., Liu, D., et al. (2018). Wilms' tumor 1-associating protein plays an aggressive role in diffuse large B-cell lymphoma and forms a complex with BCL6 via Hsp90. Cell Commun. Signal. *16*, 50.

35. Tang, J., Wang, F., Cheng, G., Si, S., Sun, X., Han, J., Yu, H., Zhang, W., Lv, Q., Wei, J.F., and Yang, H. (2018). Wilms' tumor 1-associating protein promotes renal cell carcinoma proliferation by regulating CDK2 mRNA stability. J. Exp. Clin. Cancer Res. *37*, 40.

36. Zhao, X., Chen, Y., Mao, Q., Jiang, X., Jiang, W., Chen, J., Xu, W., Zhong, L., and Sun, X. (2018). Overexpression of YTHDF1 is associated with poor prognosis in patients with hepatocellular carcinoma. Cancer Biomark. *21*, 859–868.

37. Nishizawa, Y., Konno, M., Asai, A., Koseki, J., Kawamoto, K., Miyoshi, N., Takahashi, H., Nishida, N., Haraguchi, N., Sakai, D., et al. (2017). Oncogene c-Myc promotes epitranscriptome m⁶A reader YTHDF1 expression in colorectal cancer. Oncotarget *9*, 7476–7486.

38. Tanabe, A., Tanikawa, K., Tsunetomi, M., Takai, K., Ikeda, H., Konno, J., Torigoe, T., Maeda, H., Kutomi, G., Okita, K., et al. (2016). RNA helicase YTHDC2 promotes cancer metastasis via an enhancement of the efficiency by which $HIF-1\alpha$ mRNA is translated. Cancer Lett. *376*, 34–42.

39. Lin, X., Chai, G., Wu, Y., Li, J., Chen, F., Liu, J., Luo, G., Tauler, J., Du, J., Lin, S., et al. (2019). RNA m⁶A methylation regulates the epithelial mesenchymal transition of cancer cells and translation of Snail. Nat. Commun. *10*, 2065.

40. Visvanathan, A., Patil, V., Arora, A., Hegde, A.S., Arivazhagan, A., Santosh, V., and Somasundaram, K. (2018). Essential role of METTL3-mediated m⁶A modification in glioma stem-like cells maintenance and radioresistance. Oncogene *37*, 522–533.

41. Barbieri, I., Tzelepis, K., Pandolfini, L., Shi, J., Millán-Zambrano, G., Robson, S.C., Aspris, D., Migliori, V., Bannister, A.J., Han, N., et al. (2017). Promoter-bound METTL3 maintains myeloid leukaemia by m⁶A-dependent translation control. Nature 552, 126–131.

42. Song, H., Feng, X., Zhang, H., Luo, Y., Huang, J., Lin, M., Jin, J., Ding, X., Wu, S., Huang, H., et al. (2019). METTL3 and ALKBH5 oppositely regulate m⁶A modification of *TFEB* mRNA, which dictates the fate of hypoxia/reoxygenation-treated cardiomyocytes. Autophagy 15, 1419–1437.

43. Feng, Z., Li, Q., Meng, R., Yi, B., and Xu, Q. (2018). METTL3 regulates alternative splicing of MyD88 upon the lipopolysaccharide-induced inflammatory response in human dental pulp cells. J. Cell. Mol. Med. 22, 2558–2568.

44. Chen, D., Wu, M., Li, Y., Chang, I., Yuan, Q., Ekimyan-Salvo, M., Deng, P., Yu, B., Yu, Y., Dong, J., et al. (2017). Targeting BMI1⁺ cancer stem cells overcomes chemoresist-ance and inhibits metastases in squamous cell carcinoma. Cell Stem Cell 20, 621–634.e6.

45. Dominissini, D., Moshitch-Moshkovitz, S., Salmon-Divon, M., Amariglio, N., and Rechavi, G. (2013). Transcriptome-wide mapping of N^6-methyladenosine by m⁶A-seq based on immunocapturing and massively parallel sequencing. Nat. Protoc. 8, 176–189.

46. Esposito, A.M., Mateyak, M., He, D., Lewis, M., Sasikumar, A.N., Hutton, J., Copeland, P.R., and Kinzy, T.G. (2010). Eukaryotic polyribosome profile analysis. J. Vis. Exp. 15, 40.

47. He, Q., Zhou, X., Li, S., Jin, Y., Chen, Z., Chen, D., Cai, Y., Liu, Z., Zhao, T., and Wang, A. (2013). MicroRNA-181a suppresses salivary adenoid cystic carcinoma metastasis by targeting MAPK-Snai2 pathway. Biochim. Biophys. Acta 1830, 5258–5266.